



the society for solid-state
and electrochemical
science and technology

Journal of The Electrochemical Society

Electrodeposition of Silver(II) Oxide Films

Bryan E. Breyfogle, Chen-Jen Hung, Mark G. Shumsky and Jay A. Switzer

J. Electrochem. Soc. 1996, Volume 143, Issue 9, Pages 2741-2746.
doi: 10.1149/1.1837101

**Email alerting
service**

Receive free email alerts when new articles cite this article - sign up
in the box at the top right corner of the article or [click here](#)

To subscribe to *Journal of The Electrochemical Society* go to:
<http://jes.ecsdl.org/subscriptions>

REFERENCES

1. T. Boniszewski and G. C. Smith, *Acta Metall.*, **11**, 165 (1964).
2. B. A. Wilcox and G. C. Smith, *ibid.*, **13**, 331 (1965).
3. R. M. Latanision and H. Opperhauser, Jr., *Metall. Trans.*, **5**, 233 (1975).
4. J. P. Hirth, *ibid.*, **11A**, 861 (1980).
5. C. V. Owen, T. J. Rowland, and O. Buck, *ibid.*, **16A**, 59 (1985).
6. W. A. Spitzig, C. V. Owen, and T. E. Scott, *ibid.*, **17A**, 527 (1986).
7. B. G. Pound, *Acta Metall. Mater.*, **42**, 1551 (1994).
8. M. Wall, C. E. Lane, and C. A. Hippisly, *ibid.*, **42**, 1295 (1994).
9. R. W. Revie, V. S. Sastri, G. R. Hoey, R. R. Ramsingh, D. K. Mak, and M. T. Shehata, *Corrosion*, **49**, 17 (1993).
10. H. Y. Liou, R. I. Shieh, F. I. Wei, and S. C. Wang, *ibid.*, **49**, 389 (1993).
11. S. K. Yen and H. C. Shih, *This Journal*, **137**, 2028 (1990).
12. M. A. V. Devanathan and Z. Stachurski, *Proc. R. Soc. Edinburgh, Sect. A*, **270**, 90 (1962).
13. J. McBreen, L. Nanis, and W. Beck, *This Journal*, **113**, 1218 (1966).
14. S. K. Yen and H. C. Shih, *ibid.*, **135**, 1169 (1988).
15. S.-L. Pyun and R. A. Oriani, *Corros. Sci.*, **29**, 486 (1989).
16. A. Turnbull, M. Seanz de Santa Maria, and N. D. Thomas, *ibid.*, **29**, 89 (1989).
17. J. Crank, *The Mathematics of Diffusion*, 2nd ed., p. 47, Oxford University Press, New York (1975).

Electrodeposition of Silver(II) Oxide Films

Bryan E. Breyfogle,* Chen-Jen Hung,* Mark G. Shumsky, and Jay A. Switzer**

Department of Chemistry and Graduate Center for Materials Research, University of Missouri-Rolla, Rolla, Missouri 65409-1170, USA

ABSTRACT

Continuous films of silver(II) oxide (AgO) have been electrodeposited directly from aqueous solutions of 50 mM silver acetate/25 mM sodium acetate onto 430 stainless steel, polycrystalline platinum, and indium-tin oxide-coated glass. Current efficiencies for the electrodeposition process ranged from 62 to 95% and were a function of the applied current density. X-ray diffraction of the electrodeposited films reveals a [010] texture when the thickness is greater than 1 μm . Freshly ground films or powders exhibit only reflections consistent with the monoclinic AgO structure. Rietveld analysis confirms the ground films are single-phase AgO with a P 2₁/c space group. The films were imaged and film thickness was measured by atomic force microscopy. Thermogravimetric analysis shows that the films begin to decompose in air above 130°C, with an abrupt weight loss between 180 and 200°C. The total weight loss of 6.4 to 6.5% corresponds to thermal decomposition of AgO to Ag₂O with loss of oxygen. A direct optical bandgap of 1.1 eV was measured. The black AgO films absorb strongly in the near infrared and throughout the visible region. The four-point resistivity of the AgO films was $12 \pm 1 \Omega \text{ cm}$.

Introduction

AgO has been studied extensively for its use as the cathode material in zinc-silver oxide batteries.¹ There are two common methods for preparation of AgO. One method is the electrochemical oxidation of silver metal in alkaline solutions, which results in the formation of an Ag₂O/AgO oxide layer on the metal.^{2,3} The other is by alkaline oxidation of aqueous solutions of Ag(I) salts.^{4,5} The latter technique yields a precipitate of finely divided, black, crystalline oxide, AgO.⁶ The first such preparation of AgO was performed over a century ago.⁷

Recently, nanoscale AgO particles have been synthesized by a laser vaporization/condensation method.⁸ Other recent investigations of AgO involve its use as a selective oxidizing agent for certain organic reactions⁹ and as a postchromatographic electrochemical detector for carbohydrates and amino compounds.¹⁰ AgO is used as a precursor material for the synthesis of a new family of high-*T_c* superconductors based on the Ag-Ba-Ca-Cu-O system.¹¹ AgO is also used as an additive to improve the critical current densities of Y-Ba-Cu-O-based superconductors.¹²

AgO is an especially interesting compound, as it illustrates that a simple chemical formula may not provide a complete understanding of the oxidation states and electronic configurations of the elements present. Whereas CuO contains the d⁹ ion Cu²⁺ and is paramagnetic, both the structure and properties of AgO suggest a mixed-valency compound best formulated in terms of Ag⁺(d¹⁰) and Ag³⁺(d⁸).¹³ This has been shown by magnetic measurements,¹⁴ x-ray diffraction (XRD),¹⁴ and neutron diffraction.¹⁵ In CuO all Cu atoms have four coplanar neighbors, but in AgO there are two distinct silver sites in the lattice with different coordinations and different Ag-O bond dis-

tances. Ag(I) has two colinear O neighbors with a Ag(I)-O bond distance of 2.18 Å, while the other atoms of the original square planar coordination group are at a distance of 2.66 Å. The other silver site, Ag(II), has four coplanar O neighbors at 2.05 Å.¹⁶ The crystal structure of AgO is monoclinic, space group P 2₁/c, with four formula units per unit cell. The lattice parameters measured by Scatturin *et al.* are $a = 5.85 \text{ \AA}$, $b = 3.48 \text{ \AA}$, $c = 5.50 \text{ \AA}$, and $\beta = 107.5^\circ$.¹⁵ XRD and neutron diffraction studies proposed nearly identical structures for AgO. CuO also has a monoclinic structure,¹⁶ but it belongs to the space group C 2/c.

AgO was also believed to be formed during the chemical and electrochemical oxidation of acidic and neutral solutions of Ag(I) salts. However, it was later shown that oxidation of these solutions results in the production of oxysalts of the form Ag(Ag₆O₈)X, where X = NO₃⁻, ClO₄⁻, F⁻, HSO₄⁻, HF₂⁻, and BF₄⁻.^{6,17-19} AgO powders can be produced from these oxysalts by boiling them in water,²⁰ as the oxysalts are thermally unstable.

The authors are unaware of any other studies where AgO films have been electrodeposited from Ag(I) solutions. The only previous work which involved the oxidation of a silver acetate solution was done by Selbin and Usategui,²¹ in which several silver(I) salts were oxidized with ozone. They found that the previously mentioned oxysalts were formed upon reacting ozone with AgNO₃, AgClO₄, and Ag₂SO₄, whereas with AgF and AgC₂H₃O₂, they proposed that the product of ozonation was AgO. Others who have investigated the oxidation of AgF solutions have shown the product to be the oxysalt, Ag(Ag₆O₈)F.¹⁷ This led us to investigate the product of electrochemical oxidation of AgC₂H₃O₂ solutions. We have found that we can electrodeposit AgO films directly from aqueous solutions of AgC₂H₃O₂. In this study we investigate the properties of electrodeposited AgO films by XRD, thermogravimetric analysis (TGA), four-point resistivity,

* Electrochemical Society Student Member.

** Electrochemical Society Active Member.

spectrophotometry, voltammetry, and atomic force microscopy (AFM).

Experimental

The AgO films were electrodeposited onto polycrystalline 430 stainless steel electrodes purchased from Metal Samples Co. The electrodes were mechanically polished and then ultrasonically cleaned. They were then embedded in an epoxy mold or pressed tightly into a Teflon holder and rotated at 200 rpm using a Pine AFMSRX rotator. This mounting procedure resulted in the stainless steel electrode surface being flush with the epoxy or Teflon surface. The areas of the polished stainless steel electrodes were either 1.98 or 3.83 cm². All solutions were made from reagent-grade chemicals dissolved in doubly distilled deionized water from a Barnstead-NANOpure Ultra Pure water system. The silver acetate solutions were filtered before each deposition to remove any precipitate. The solutions from which the AgO films were deposited were 50 mM AgC₂H₃O₂ and 25 mM NaC₂H₃O₂. The solutions were bubbled with nitrogen prior to and during the electrodeposition process. These solutions were light and air sensitive, and therefore new solutions were prepared daily. It was found that if the solutions were not bubbled with nitrogen and/or were used for more than several hours, an Ag₂CO₃ impurity became apparent upon analysis of the films and powders. Electrochemical depositions and cyclic voltammograms were performed using an EG&G Princeton Applied Research Model 273A potentiostat/galvanostat. All depositions were performed at 25°C using a controlled temperature water bath attached to a water-jacketed beaker. The cell configuration consisted of a standard three-electrode arrangement with the counterelectrode placed horizontally approximately 1 cm below a horizontal working electrode. A silver wire was used as the reference electrode. All the films grown for this study were deposited at 0.25 mA/cm². This current density was chosen because a high current efficiency and an appreciable deposition rate could be obtained. After the AgO films were grown to the desired thickness, they were thoroughly rinsed with deionized water, dried with nitrogen, and placed in a desiccator.

XRD patterns of the electrodeposited AgO films and powders produced from ground films were run on a Scintag 2000 diffractometer using Cu K_α radiation ($\lambda = 1.54178 \text{ \AA}$). The x-ray tube was operated at an accelerating voltage of 45 kV and an emission current of 40 mA. XRD experiments on AgO films were performed with the films deposited on the 430 stainless steel electrodes. AgO powders were produced by removing the films from the electrodes and grinding them for several minutes with a mortar and pestle. Due to the small amount of powder available, standard sample holders for the x-ray diffractometer could not be used. Therefore, the ground films were dispersed on glass for XRD experiments. This method was also used for XRD of powders before and after TGA. TGA experiments were performed in air on a Perkin-Elmer Model TGS-2 TGA. Powdered samples of 10–15 mg were used. The samples were heated at 5 °C/min in Pt pans to the desired temperature, after which they were cooled to room temperature at 40 °C/min. AFM images of the films were obtained with a Nanoscope E (Digital Instruments) using Si₃N₄ cantilevers. AgO film thicknesses were measured in the AFM by etching a step edge in the film with dilute nitric acid and then measuring the height difference between the substrate and the surface of the film. The z direction in the AFM was calibrated with a 1 μm height standard before measuring film thicknesses. Resistivity measurements of the AgO films were obtained by the four-point method using an Alessi four-point probe in conjunction with a Keithley Model 181 nanovoltmeter and Model 220 programmable current source. Resistivity measurements were made on free-standing films which peeled off the electrode and on films which were removed by placing adhesive on a glass slide and pulling off the AgO films.

Results and Discussion

A cyclic voltammogram for an uncoated Pt electrode in the deposition solution with a silver reference electrode and a scan rate of 20 mV/s is shown in Fig. 1. The loops at the ends of the voltammogram are indicative of three-dimensional nucleation and growth, since the electrochemically active surface area of the electrode increases due to the formation of three-dimensional deposits.¹⁸ There are also crossovers in the voltammogram at 0 and 0.6 V vs. Ag. We attribute these crossovers to the stripping of electrodeposited Ag metal and AgO, respectively. Hence, as the potential is driven negative, Ag metal deposition occurs at about -0.07 V, with subsequent stripping when the potential is driven positive of 0 V. The deposition of AgO begins at very low current density just positive of the Ag stripping peak and begins to increase rapidly at about 0.6 V. Stripping of the AgO begins as the potential is driven negative of the crossover at 0.6 V and reaches a maximum at about 0.25 V. The charge under the AgO stripping peak was always less than the charge passed during the sweep to positive potentials and anodic current densities.

During AgO deposition at current densities in the 0.5 mA/cm² range, gas evolution is obvious at the electrode surface. We attribute this gas evolution to a parasitic oxygen evolution reaction. In agreement with this interpretation, the current efficiency for AgO deposition decreases with increasing applied potential or anodic current density. A plot of current efficiency vs. current density is shown in Fig. 2. The current efficiencies were determined gravimetrically. The current efficiency decreases from 95% at a current density of 0.1 mA/cm² to 62% at 1.0 mA/cm². A deposition current density of 0.25 mA/cm² was used to deposit the films for characterization in this study, since the current efficiency was approximately 92%.

A linear sweep voltammogram for an AgO-coated Pt electrode in the deposition solution is shown in Fig. 3. The AgO coating had a nominal thickness of 0.1 μm based on Faraday's Law. The open-circuit potential of the AgO electrode in this solution is 0.37 V vs. Ag. The current densities measured from this voltammogram give a good indication of what potential must be applied to achieve a desired steady-state deposition current density and corresponding current efficiency (from Fig. 2).

It is interesting that AgO deposits from AgC₂H₃O₂ solutions rather than the oxysalt which deposits from other Ag(I) salts. Table I lists the anode products of different Ag(I) salts. The ionic radii in Table I are thermochemical radii, calculated by Jenkins and Thakur.²² This table suggests that the pK_a of the anion is a more important factor than its size in determining whether the anion will be

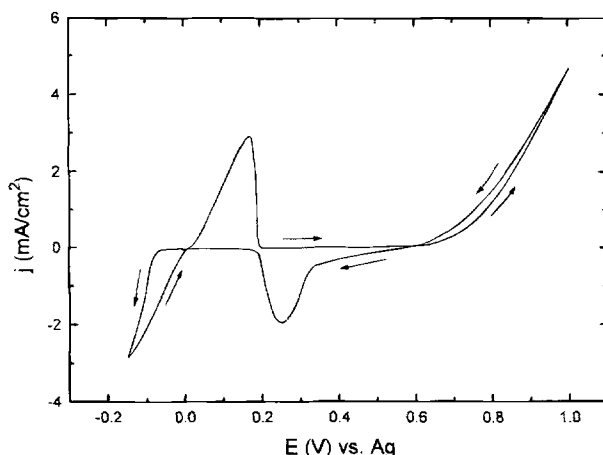


Fig. 1. Cyclic voltammogram for an uncoated Pt electrode in 50 mM AgC₂H₃O₂/25 mM NaC₂H₃O₂ solution in the potential range -0.15 to 1.0 V vs. Ag. The arrows indicate scan direction. The area of the Pt electrode is 0.138 cm² and the scan rate is 20 mV s⁻¹.

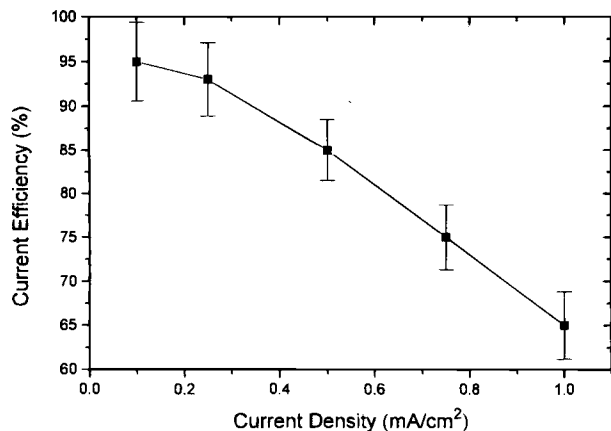


Fig. 2. Current efficiency, measured gravimetrically, as a function of applied current density. Error bars indicate the uncertainty for each given measurement.

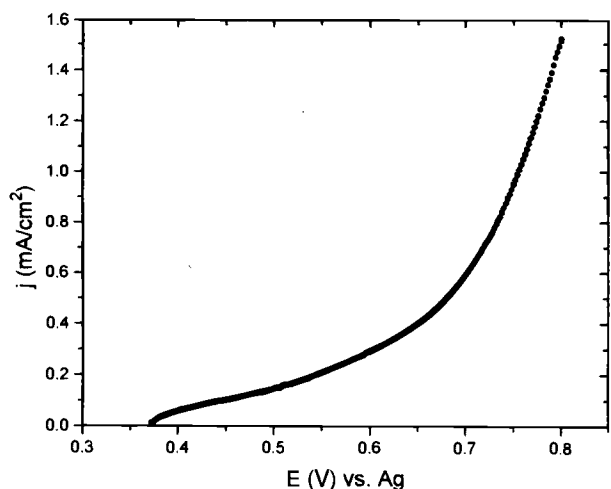


Fig. 3. Linear sweep voltammogram for a thin AgO film on Pt in the potential range 0.37 V (the open-circuit potential of the AgO film) to 0.8 V vs. Ag, scan rate 20 mV s⁻¹.

incorporated into the lattice of the anode product, since the anions with high pK_a will tend to be protonated due to the low surface pH during oxide formation.

X-ray diffraction of AgO deposits.—XRD was used to characterize the deposits grown from a 50 mM Ag₂H₃O₂/25 mM NaC₂H₃O₂ solution at 0.25 mA/cm² on 430 stainless steel electrodes. Figure 4a shows an XRD pattern for a 5 μm thick AgO film that was grown on 430 stainless steel. The only Bragg reflection apparent for AgO in this pattern is the (020) reflection at 2θ = 52.3°. The high intensity of this reflection relative to others normally apparent for AgO in this range of 2θ values is indicative of a strongly preferred orientation or texture for the film. In this case it indicates that the (010) planes for AgO are parallel to the substrate surface. Figure 4b shows the XRD pattern for a powder made from grinding several films like the one in Fig. 4a. Figure 4c shows a stick diagram for JCPDS Card No. 22-472 for AgO. It is apparent by comparing Fig. 4b

Table I. Anions of some Ag(I) salts with anion pK_a, thermochemical radii, and anode product from aqueous solutions of the Ag(I) salt.

Anion	Radius (Å)	pK _a	Anode product
ClO ₄ ⁻	2.40	-7	Ag(Ag ₆ O ₈)ClO ₄
NO ₃ ⁻	1.79	-1.3	Ag(Ag ₆ O ₈)NO ₃
F ⁻	1.26	3.18	Ag(Ag ₆ O ₈)F
C ₂ H ₃ O ₂ ⁻	1.62	4.75	AgO

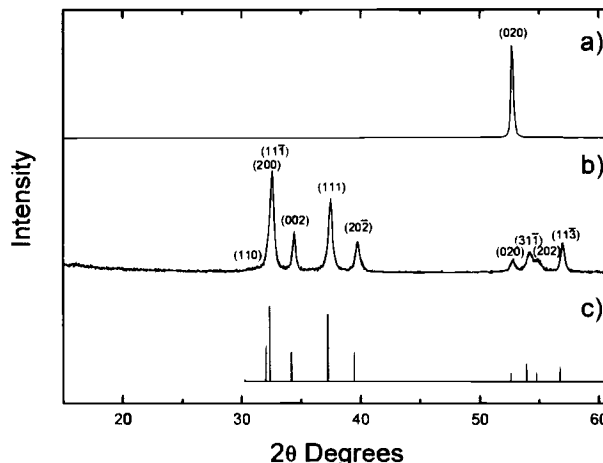


Fig. 4. XRD patterns of: (a) 5 μm thick, [010]-textured AgO film, deposited from 50 mM Ag₂H₃O₂/25 mM NaC₂H₃O₂ at 0.25 mA/cm² on 430 stainless steel; (b) AgO powder produced by pulverizing several films; and (c) JCPDS Card No. 22-472 for AgO.

and c that the material produced from our electrodeposition is consistent with AgO. It was important that the films and powders were produced from freshly prepared, nitrogen-purged solutions, and that the x-ray analysis was performed on freshly deposited AgO. If the solutions, films, or powders were allowed to age, impurities began to become apparent in the films and powders. The main impurity present was Ag₂CO₃. Trace amounts of carbonate were always apparent by infrared (IR) absorption spectroscopy. Some residual water is also evident in the IR spectra. Carbon and hydrogen analysis of the AgO powders are consistent with trace amounts of carbonate and water. The silver carbonate impurity was not evident in XRD of fresh films or powders; however, as the powders aged, it became a major impurity. This increase with age indicates that Ag₂CO₃ is a degradation product of AgO. Ag₂CO₃ was also present as an impurity in commercially available AgO powders that we analyzed. An XRD pattern for our AgO powder exposed to air for 5 months is shown in Fig. 5a. Fig 5b and c are stick diagrams of JCPDS cards 26-339 and 22-472 for Ag₂CO₃ and AgO, respectively.

A Rietveld refinement²³ was performed on the experimental data in Fig. 4b to determine the fit of this data to the AgO structure. Table II shows the atomic positions obtained for AgO by refinement in the P 2₁/c space group. The values obtained are within experimental error identical with those of Ref. 15. The fit of the refined structure to the experimental data is shown in Fig. 6 with R_e = 8.0%

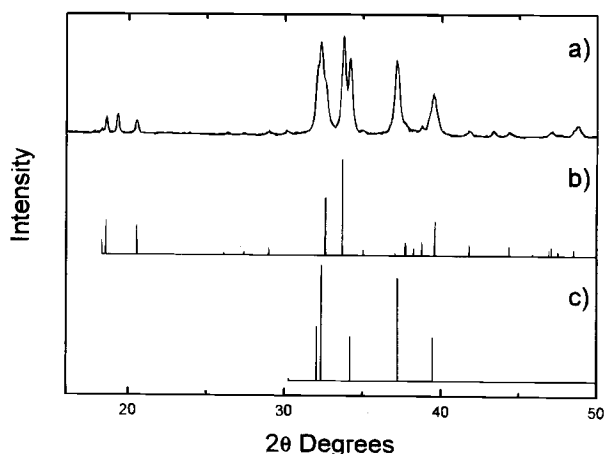


Fig. 5. XRD patterns of: (a) AgO powder produced from pulverized films after exposure to air for 5 months; (b) JCPDS Card No. 26-339 for Ag₂CO₃; and (c) JCPDS Card No. 22-472 for AgO.

Table II. Atomic positions for monoclinic AgO, space group P 2₁/c.

Atom	<i>x</i>	<i>y</i>	<i>z</i>
O	0.295	0.344	0.229
Ag(I)	1/2	0	1/2
Ag(III)	0	0	0

Cell parameters: *a* = 5.85 Å, *b* = 3.49 Å, *c* = 5.50 Å; β = 107.4°.

and R_{wp} = 11.3%. Some of the slight discrepancies in intensities may be due to the small amount of AgO powder from which the XRD pattern was taken.

Thermogravimetric analysis of AgO deposits.—AgO is known to decompose to Ag₂O at temperatures above 100 °C.²⁴ At higher temperatures, the decomposition product is metallic silver. TGA was performed in air on powdered samples of the electrodeposited AgO films to assess their decomposition behavior. Figure 7 shows TGA data for the AgO powder from 30 to 250°C. At the heating rate of 5°C/min, the powder begins to lose mass noticeably at temperatures greater than 130°C, with a sharp decline centered at about 190°C. The weight percent change of 6.44% corresponds well with the 6.46% weight loss associated with the following decomposition reaction

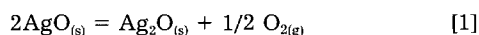


Figure 8a shows the XRD pattern for the AgO powder before TGA. The powder pattern is in good agreement with the stick diagram of JCPDS Card No. 22-472 for AgO shown in Fig. 8b. The intensity of the (020) peak for our powder is higher than that in JCPDS stick diagram as a result of insufficient grinding of the [010]-textured AgO films. Figure 8c shows the XRD pattern for the powder after being heated to 250°C and then cooled back to room temperature during the TGA experiment. The Bragg peaks in this pattern agree with those of JCPDS Card No. 12-793 for Ag₂O, as shown in Fig. 8d. If the TGA experimental temperature was allowed to go higher than 250°C, metallic silver became apparent both by microscopic analysis and XRD. These results emphasize the advantage of electrodeposition for producing materials in unusual oxidation states at low temperature.

AFM of AgO films.—An AFM image of a [010]-textured AgO film is shown in Fig. 9. The image shows that elec-

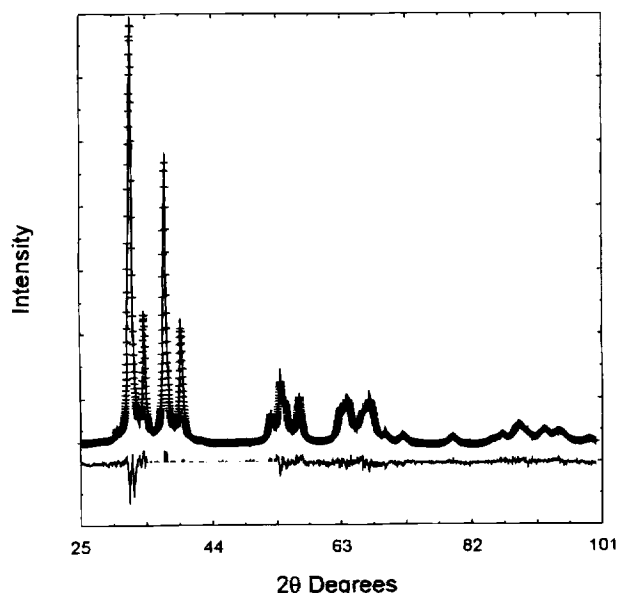


Fig. 6. Rietveld refinement for AgO powder produced at 0.25 mA/cm²: (—) experimental data, (+) refined pattern. A difference pattern is shown below the fit.

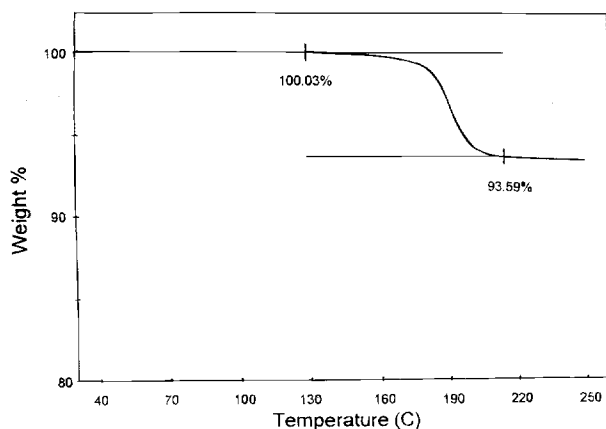


Fig. 7. TGA of AgO powder in air in the temperature range 30 to 250°C showing weight loss of 6.44% between 130 to 215°C. Sample weight 13.6698 mg, heating rate 5.00°C/min.

trodeposited AgO grows as an apparently dense film with grain sizes on the order of 0.1 to 0.5 μm. AFM measurements were also employed to measure the thickness of our electrodeposited AgO films. A step was etched in the films by placing them in dilute nitric acid until the submerged portion of the film was completely dissolved. The films were then placed in the AFM and the difference in height from the substrate to the surface of the film was measured. Before these measurements were made, a 1 μm height standard was used to calibrate the *z* direction in the AFM. Figure 10 shows an AFM image for an etched AgO film. The observed height of 1.2 ± 0.1 μm agrees with the film thickness calculated by Faraday's law using the density of AgO (7.44 g/cm³) and assuming 100% current efficiency. Since the actual current efficiency is 92% at this deposition current density, these results suggest that there may be some porosity in the films (*i.e.*, the density is less than 7.44 g/cm³). The uncertainty in the AFM measurement of height, however, precludes determination of porosity by this method. This measured film thickness was then used in determining the electrical resistivity of the electrodeposited AgO films by four-point resistivity measurements. The measured resistivity of the films was 12 ± 1 Ω cm. This is in good agreement with resistivities previously measured on pellets of pressed AgO powder of 10 and 14.3 Ω cm.^{25,26}

Optical absorption measurements for AgO films.—Although AgO is often referred to as a semiconductor based on its electrical resistivity, there are no literature values given for its bandgap. Therefore, we attempted to measure the bandgap of the AgO films by optical absorp-

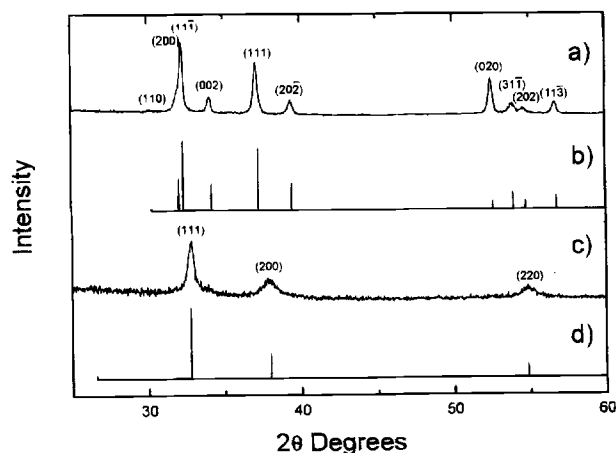


Fig. 8. XRD patterns of: (a) AgO powder before TGA, (b) JCPDS Card No. 22-472 for AgO, (c) decomposed powder after heating in TGA, and (d) JCPDS Card No. 12-793 for Ag₂O.

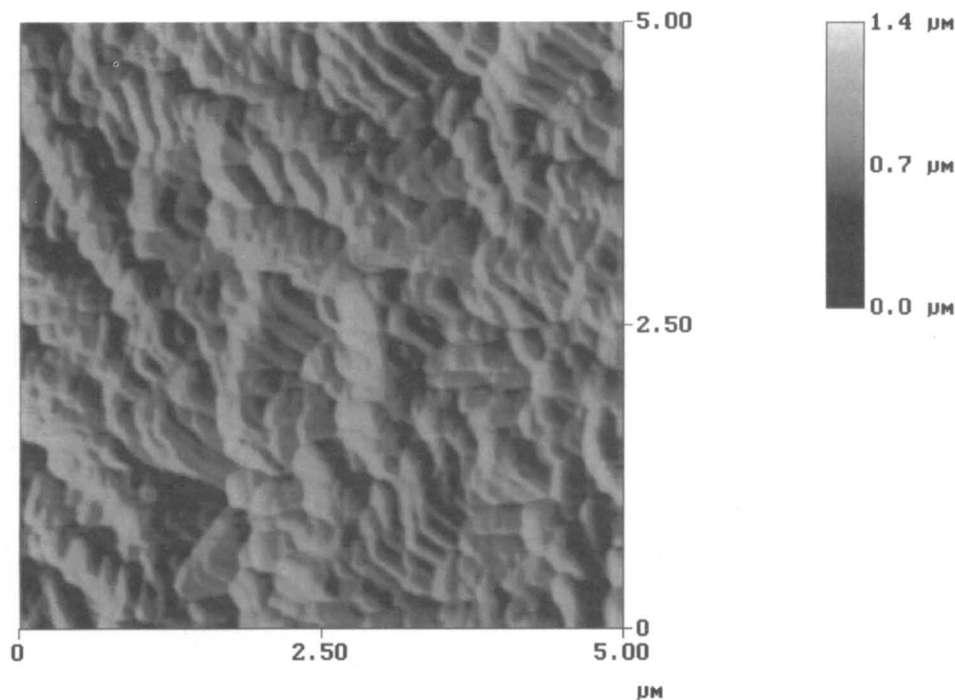


Fig. 9. Top view AFM image showing morphology of a 5 μm thick AgO film deposited from 50 mM $\text{Ag}_2\text{C}_2\text{H}_3\text{O}_2$ /25 mM $\text{Na}_2\text{C}_2\text{H}_3\text{O}_2$ at 0.25 mA/cm² on 430 stainless steel.

tion methods.²⁷ An absorption spectrum for a 1 μm thick AgO film on indium-tin oxide (ITO) coated glass is shown in Fig. 11. The absorption of the AgO films increases dramatically between 1250 and 900 nm. The absorption coefficient, α , was determined from²⁸

$$e^{-\alpha t} = T/(1 - R)^2 \quad [2]$$

where t is the thickness, and T and R are the transmittance and specular reflectance of the film, respectively. However, since the specular reflectance of the AgO film is virtually zero in this range, the expression can be simplified as follows

$$e^{-\alpha t} = T \quad [3]$$

A plot of $(\alpha E)^2$ vs. E for a 1 μm thick AgO film electrodeposited on ITO-coated glass is shown in Fig. 12. A linear relationship for this plot indicates a direct bandgap for the

absorbing material.²⁷ As seen in Fig. 12 there is appreciable low energy tailing of the spectrum. The direct bandgap measured by this method is 1.1 eV.

We have electrodeposited AgO as continuous films directly from aqueous solutions of silver acetate. The fact that AgO forms, instead of a silver oxysalt of the anion, is likely due to a pK_a effect rather than anion size. The highly textured nature of the films, along with the known non-stoichiometry of AgO^{14} , make it an ideal candidate for growth of defect-chemistry superlattices.²⁹ A direct bandgap of 1.1 eV was measured by an optical absorption technique. XRD, TGA, and electrical resistivity measurements on the films are all consistent with measurements obtained previously on AgO powders.

Acknowledgments

This work was supported in part by the Division of Materials Research of the National Science Foundation,

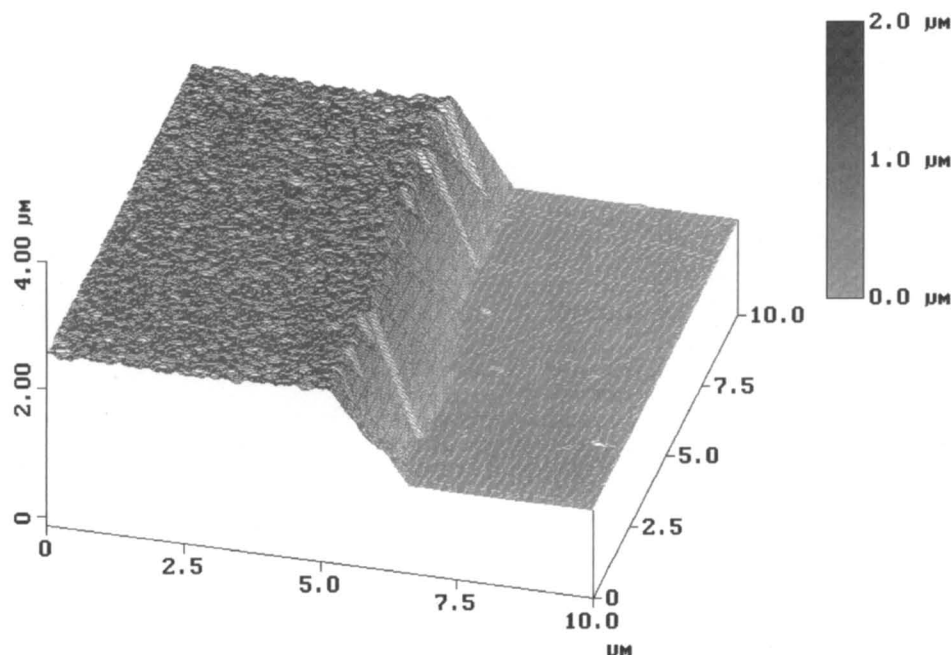


Fig. 10. Top view AFM line drawing of a 1.2 μm thick AgO film. A step edge has been etched in the film with dilute HNO_3 . The thickness of the film was then measured by the displacement in the z direction between the substrate and the surface of the film.

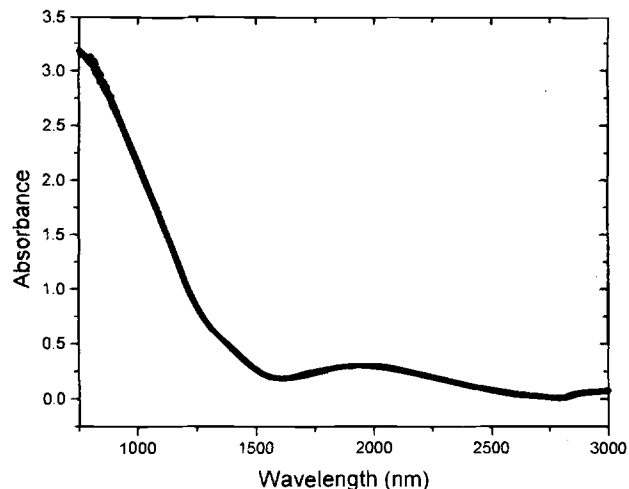


Fig. 11. Optical absorption spectrum for a 1 μm thick AgO film deposited on ITO-coated glass from 50 mM $\text{AgC}_2\text{H}_3\text{O}_2$ /25 mM $\text{NaC}_2\text{H}_3\text{O}_2$ at 0.25 mA/cm², scan rate 200 nm/min.

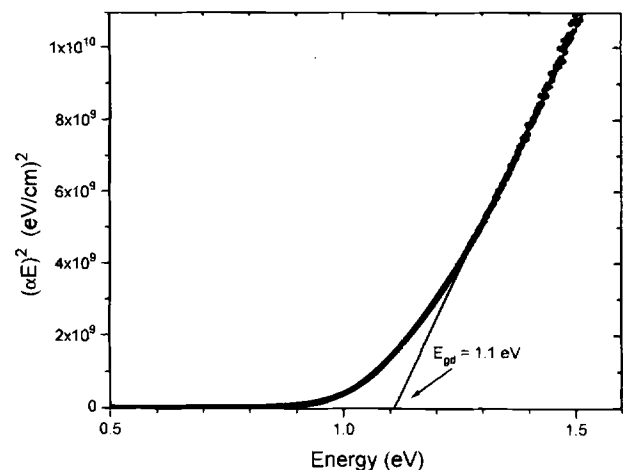


Fig. 12. Plot of $(\alpha E)^2$ as a function of energy. The region between 1.25 and 1.50 eV is linear and indicates a direct transition from the valence band to the conduction band. The energy-intercept of the fit to the linear region gives a direct optical bandgap of 1.1 eV.

Grant No. DMR-9202872, the Materials Division of the Office of Naval Research, Grants N00014-91-J-1499 and N00014-94-1-0917, and the University of Missouri Research Board.

Manuscript submitted Jan. 11, 1996; revised manuscript received May 29, 1996.

University of Missouri-Rolla assisted in meeting the publication costs of this article.

REFERENCES

1. *Zinc-Silver Oxide Batteries*, A. Fleischer and J. L. Landers, Editors, The Electrochemical Society Monograph Series, John Wiley & Sons, New York (1971).
2. T. Dirske, *This Journal*, **106**, 920 (1959).
3. C. P. Wales and J. Burbank, *ibid.*, **106**, 885 (1959).
4. *Inorganic Synthesis IV*, J. C. Bailar, Jr., Editor, p. 4, McGraw-Hill Book Co., New York (1953).
5. A. N. Mansour and S. Dallek, *This Journal*, **137**, 1467 (1990).
6. J. A. McMillan, *Chem. Rev.*, **62**, 65 (1962).
7. J. Schiel, *Liebig's Ann.*, **132**, 322 (1864).
8. M. Samy El-Shall, W. Slack, D. Hanley, and D. Kane, *Mater. Res. Soc. Symp. Proc.*, **351**, 369 (1994).
9. M. Hisatome, J. Watanabe, and K. Yamakawa, *Bull. Chem. Soc. Jpn.*, **67**, 280 (1994).
10. T. P. Tougas, M. J. DeBenedetto, and J. M. Demott, Jr., *Electroanalysis*, **5**, 669 (1993).
11. H. Ihara, K. Tokiwa, H. Ozawa, M. Hirabayashi, H. Matuhata, A. Negishi, and Y. S. Song, *Jpn. J. Appl. Phys.*, **33**, L300 (1994).
12. C. Y. Huang, H. H. Tai, and M. K. Wu, *Mod. Phys. Lett. B*, **3**, 525 (1989).
13. P. A. Cox, *Transition Metal Oxides-An Introduction to Their Electronic Structure and Properties*, International Series of Monographs on Chemistry, Vol. 27, p. 117, Clarendon Press, Oxford (1995).
14. J. A. McMillan, *J. Inorg. Nucl. Chem.*, **13**, 28 (1960).
15. V. Scatturin, P. L. Bellon, and A. J. Salkind, *This Journal*, **108**, 819 (1961).
16. A. F. Wells, *Structural Inorganic Chemistry*, 5th ed., p. 1103, Oxford University Press, New York (1991).
17. M. B. Robin, K. Andres, T. H. Geballe, N. A. Kuebler, and D. B. McWhan, *Phys. Rev. Lett.*, **17**, 917 (1966).
18. G. D. Adzic, A. R. Despic, and D. M. Drazik, *J. Electroanal. Chem.*, **241**, 353 (1988).
19. B. E. Breyfogle, R. J. Phillips, and J. A. Switzer, *Chem. Mater.*, **4**, 1356 (1992).
20. W. L. Jolly, *The Synthesis and Characterization of Inorganic Compounds*, p. 37, Prentice-Hall, Englewood Cliffs, NJ (1970).
21. J. Selbin and M. Usategui, *J. Inorg. Nucl. Chem.*, **20**, 91 (1961).
22. H. D. B. Jenkins and K. P. Thakur, *J. Chem. Educ.*, **56**, 576 (1979).
23. R. A. Young, in *The Rietveld Method*, R. A. Young, Editor, Chap. 1, Oxford University Press (1995).
24. M. C. Snead, J. L. Meynard, and R. C. Brasted, *Comprehensive Inorganic Chemistry*, Vol. II, D. Van Nostrand Company, Inc., New York (1954).
25. M. LeBlanc and H. Sachse, *Physik. Z.*, **32**, 887 (1931).
26. A. B. Neiding and I. A. Kazarnovskii, *Doklady Akad. Nauk SSSR*, **78**, 713 (1951).
27. R. A. Van Leeuwen, C.-J. Hung, D. R. Kammler, and J. A. Switzer, *J. Phys. Chem.*, **99**, 15247 (1995).
28. J. I. Pankove, *Optical Processes in Semiconductors*, Dover, New York (1975).
29. J. A. Switzer, C.-J. Hung, B. E. Breyfogle, M. G. Shumsky, R. A. Van Leeuwen, and T. D. Golden, *Science*, **264**, 1573 (1994).